

Many-body enhancement in a spin-chain quantum heat engine

L. A. Williamson¹ and Matthew J. Davis¹

¹*ARC Centre of Excellence for Engineered Quantum Systems, School of Mathematics and Physics,
University of Queensland, St Lucia, Queensland 4072, Australia*

(Dated: February 6, 2023)

We show that ferromagnetic interactions can enhance the adiabatic performance of a quantum spin chain engine at low temperatures. The enhancement in work output is particularly pronounced, increasing exponentially with interaction strength. The performance enhancement occurs in the paramagnetic phase and is qualitatively explained by considering just the ground and first excited state, in which case the system exhibits bipartite entanglement. As the temperature is increased, thermal occupation of higher energy levels diminishes performance. We find that these thermal fluctuations are smallest for long-range interactions, resulting in the highest efficiency. Diabatic work extraction degrades performance due to quantum friction. We identify an approximate, experimentally realisable counterdiabatic drive that can mitigate friction for weak interactions.

Quantum heat engines convert heat into work utilising some distinctly quantum effect in the reservoir or working substance [1]. Reservoirs possessing coherence [2–4], squeezing [5–11] or entanglement [12, 13] have been shown to improve engine performance. Coherence in a working substance can be utilised as a resource [14–17] and can improve power output for rapid engine cycles [18, 19]. In the many-body regime, interactions in a Bose gas can enhance engine performance compared to a non-interacting gas [20–23]. Interactions in a many-body quantum system can also be tuned to change the energy of a working substance, hence providing a means to extract work [24, 25].

One of the simplest quantum working substances is an ensemble of two-level systems (“spins”) [19, 26–35]. Work can be extracted by tuning the level spacing $\hbar\omega(t)$ via control of an external field, see Fig. 1(a). Including interactions between spins opens up the possibility to explore many-body quantum effects. While considerable work has explored engines with two interacting spins [36–47], much less is known about higher numbers of spins. For nearest-neighbour interactions, a spin chain can function as both a heat engine and a refrigerator [48] with critical scaling of performance close to the critical point [49]. However, the question of whether many-body effects can improve the performance of a spin-chain quantum heat engine has not been explored.

In this work we characterise the performance of an Otto cycle with a ferromagnetic spin chain as the working substance. In addition to displaying rich many-body physics, this system may be realised in experiments with a remarkable degree of control [50–54]. We show that both short and long-range interactions improve the adiabatic work output and efficiency in the paramagnetic phase at low temperatures $k_B T \lesssim \hbar\omega$. The performance enhancement is qualitatively explained by an analytic model considering just the ground and first excited state, in which case the thermal state exhibits bipartite entanglement. For temperatures $k_B T > \hbar\omega$, higher energy eigenstates are occupied and the performance degrades,

approaching the non-interacting performance. This effect is reduced as the range of interactions is increased, and hence high efficiency is most robust for long-range interactions. For diabatic work extraction, decreasing the engine cycle time decreases performance due to quantum friction [36, 37, 55]. We demonstrate an approximate, experimentally realisable counterdiabatic drive that can mitigate friction for weak interactions, and hence a performance enhancement is possible at finite power output.

System setup. A chain of N ferromagnetic interacting two-level spins is described by the Hamiltonian (hereon $\hbar \equiv 1$),

$$\hat{H}(\omega(t)) = -\omega(t) \sum_{i=1}^N \hat{\sigma}_z^{(i)} - g \sum_{\substack{i,j=1 \\ (j \neq i)}}^N J_{ij} \hat{\sigma}_x^{(i)} \hat{\sigma}_x^{(j)}, \quad (1)$$

with $\hat{\sigma}_\mu^{(i)}$ ($\mu = x, y, z$) the Pauli spin-1/2 matrices for spins $i = 1, \dots, N$. The interaction strength between spins i and j is gJ_{ij} with $J_{ij} = 1/|i - j|^p$, $g \geq 0$ the nearest-neighbour interaction strength and $p > 0$ determining the range of interactions, with both g and p tuneable in experiments [51, 53]. For $N \rightarrow \infty$, the system may be ferromagnetic ($g \lesssim \omega$) or paramagnetic ($g \gtrsim \omega$) with the precise cross-over $g_c(p)$ dependent on p [56–62]. We denote nearest-neighbour interactions by $p = \infty$.

We consider an Otto engine cycle with the following steps, as shown in Fig. 1(a). (1) We begin with a hot thermal state $\rho_H^{\text{th}} = e^{-\beta_H \hat{H}(r\omega_0)} / Z(\beta_H, r\omega_0)$ at level spacing $\omega = r\omega_0$, with $r > 1$ the “compression ratio” [63], $Z(\beta, \omega) = \text{Tr} e^{-\beta \hat{H}(\omega)}$ the partition function, and $\beta = (k_B T)^{-1}$ the inverse temperature. (1 \rightarrow 2) The system is then thermally isolated and work is extracted by decreasing ω from $r\omega_0$ to ω_0 , via the protocol $\omega(t)/\omega_0 = f(t) = r + (1 - r) \sin^2(\pi t/2\tau)$ ($0 \leq t \leq \tau$). (2 \rightarrow 3) Next, we cool the system at fixed $\omega = \omega_0$, leaving the system in a cold thermal state $\rho_C^{\text{th}} = e^{-\beta_C \hat{H}(\omega_0)} / Z(\beta_C, \omega_0)$. (3 \rightarrow 4) We thermally isolate the system again and increase ω from ω_0 back to $r\omega_0$, with the protocol $\omega(t)/\omega_0 = f(\tau - t)$ ($0 \leq t \leq \tau$). (4 \rightarrow 1) Finally we heat the system at fixed

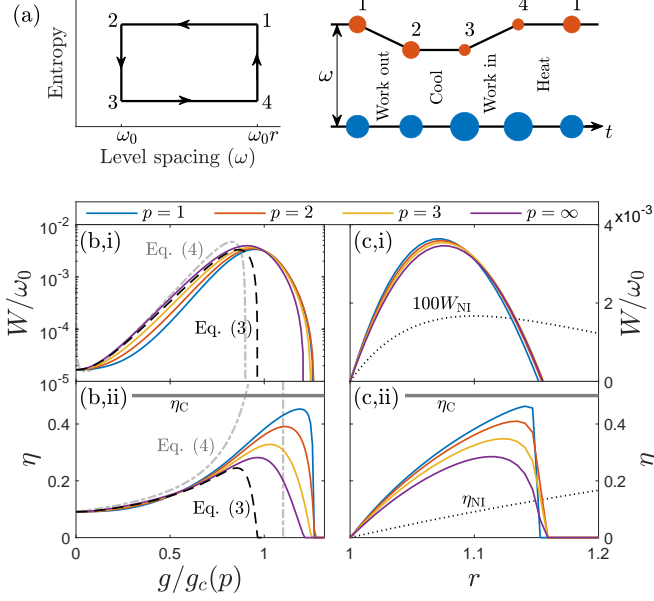


FIG. 1. (a) An Otto cycle can be realised in an ensemble of two-level spins, as described in the main text. Area of blue and red spots indicate relative ground and excited state occupations, respectively. (b),(c) Engine performance for a 10-spin chain operating adiabatically at low temperature ($\beta_H = 10\omega_0^{-1}$, $\beta_C = 2\beta_H$). Increasing g increases both (b,i) work output and (b,ii) efficiency, with maximum performance at $g \approx g_c(p)$ (results for $r = r_{\text{NI}}^{\text{max}}$). Above this, the system transitions to the ferromagnetic phase and no longer functions as an engine. For $p = \infty$, the behaviour is captured by Eq. (3) (black dashed line) and the approximation Eq. (4) (gray dot-dashed line). (c,i) Work output and (c,ii) efficiency as a function of compression ratio for $g = g_c(p)$, with dotted lines indicating the non-interacting results W_{NI} and η_{NI} (W_{NI} is scaled by a factor of 100). Gray horizontal lines in (b,ii),(c,ii) is the Carnot efficiency.

$\omega = r\omega_0$ back to the initial state. The work output W and efficiency η of the engine cycle are

$$W = Q_H - Q_C, \quad \eta = \frac{W}{Q_H}. \quad (2)$$

Here $Q_H = \text{Tr} [\hat{H}(r\omega_0)(\rho_H^{\text{th}} - \rho_4)]$ is the heat input from the hot reservoir and $Q_C = -\text{Tr} [\hat{H}(\omega_0)(\rho_C^{\text{th}} - \rho_2)]$ is the heat output to the cold reservoir, with ρ_4 the density matrix prior to coupling to the hot reservoir and ρ_2 the density matrix prior to coupling to the cold reservoir. The density matrix at points 2 and 4 are obtained by time-evolving the von Neumann equation $\dot{\rho}(t) = -i[H(t), \rho(t)]$ with initial conditions ρ_H^{th} and ρ_C^{th} respectively, using Runge-Kutta integration.

Adiabatic low-temperature performance. We first examine the quantum adiabatic limit $\tau \gg \omega_0^{-1}, g^{-1}$ (we set $\tau = 100\omega_0^{-1}$) such that transitions between eigenstates during the work steps are suppressed [64–67]. For zero in-

teractions and fixed $\beta_H\omega_0 \gg 1$, the maximum work output occurs at a compression ratio $r_{\text{NI}}^{\text{max}} \approx 1 + (\beta_H\omega_0)^{-1}$, which gives a small efficiency $\eta_{\text{NI}} \approx (\beta_H\omega_0)^{-1}$ that decreases with decreasing temperature. We find that interactions drastically improve both work output and efficiency in the paramagnetic phase for temperatures $\beta_H^{-1} \ll \omega_0$, see Fig. 1(b). The improvement in work output is particularly pronounced, with a maximum work output $\sim 10^2$ times larger than the non-interacting ensemble.

The behaviour is qualitatively similar in all cases $p = 1, 2, 3, \infty$ after rescaling interactions by $g_c(p)$, which we define to be the point at which $\partial^2 \Delta / \partial g^2|_{\omega=\omega_0}$ has a maximum [68]. Here Δ is the energy gap to the first excited state. The improvement increases monotonically up to $g \approx g_c(p)$, before dropping abruptly. For $p = 2, 3, \infty$ the performance scales approximately extensively with increasing N [68]. For $p = 1$ the performance increases non-extensively [68] due to the non-extensive thermodynamics of long-range interactions [69, 70]. This is removed after scaling g by g_c [68].

In the limit of large N , a chain with nearest neighbour interactions has a solvable spectrum [71]. For $\beta_H^{-1} \ll \omega_0, g$, only the first N excited states are appreciably occupied. The dimensionless free energy is then [72]

$$\ln Z \approx \frac{N}{\pi} \int_0^\pi e^{-\beta \sqrt{\omega^2 + g^2 - 2\omega g \cos \theta}} d\theta. \quad (3)$$

The performance computed from Eq. (3) (see [68]) is plotted alongside the full numerical results in Fig. 1(b), and agrees well with the $p = \infty$ results for $g < g_c$. Transforming the spin operators using a Holstein-Primakoff transformation and expanding to quadratic order in the bosonic operators gives an analytically tractable theory even for long-range interactions [73]. To lowest order in g/ω and for large N and β , $\ln Z \approx N\mathcal{G}_p(\beta g)e^{-\beta\Delta}$, where $N e^{-\beta\Delta}$ is the low-temperature free energy of N two-level systems with level splitting $\Delta(\omega) = \omega(1 - \omega_0 g / \omega g_c)$. The factor $\mathcal{G}_p(\beta g)$ arises from thermal fluctuations and depends on p [68]. To lowest order in β^{-1} , this gives,

$$W = N(r-1)\omega_0\mathcal{G}_p(\beta_H g) \left(e^{-\beta_H \Delta(r\omega_0)} - e^{-\beta_C \Delta(\omega_0)} \right),$$

$$\eta = 1 - \frac{\Delta_2}{\Delta_1}. \quad (4)$$

For $g < g_c(p)$, increasing g decreases $\Delta(\omega)$. From examination of Eq. (4), this increases low-temperature work output as $W \sim W_{\text{NI}} e^{\beta_H \omega_0 g / g_c}$, consistent with the exponential increase in Fig. 1(b,i), and efficiency as $\eta \sim \eta_{\text{NI}} / (1 - g / r g_c)$. Above g_c the system transitions to the ferromagnetic state and Δ , and therefore $\partial^2 \ln Z / \partial \beta \partial \omega$, changes sign. The cycle therefore no longer functions as a heat engine [48], resulting in the abrupt drop in performance in Fig. 1(b) above g_c .

The quadratic approximation above permits a calculation of the bipartite entanglement of the spin chain,

which allows us to determine the “quantum” nature of the performance enhancement. For low temperatures, a thermal state can be approximated by $\rho_T^{01} \approx (|0\rangle\langle 0| + e^{-\beta\Delta}|1\rangle\langle 1|)/(1 + e^{-\beta\Delta})$, with $|0\rangle$ the ground state, $|1\rangle = \sum_{i=1}^N \hat{\sigma}_+^{(i)}|0\rangle/\sqrt{N}$ the approximate first-excited state (independent of p) and $\hat{\sigma}_+^{(i)} = \hat{\sigma}_x^{(i)} + i\hat{\sigma}_y^{(i)}$ [68]. In [68], we show that ρ_T^{01} is entangled according to the Peres-Horodecki criterion [74–76]. The performance enhancement, Eq. (4), requires access to an entangled thermal state, and so is a many-body quantum effect. The entanglement of $|1\rangle$ is also directly evident from the entanglement entropy, which is $\mathcal{S} = \ln(N/2)$ for a partition dividing the spin chain in half [68]. In contrast, in a mean-field approximation, the interaction of spin i with the remaining spins is replaced by $-g\Omega_i\hat{\sigma}_x^{(i)}$. Here $\Omega_i = \sum_{j \neq i} J_{ij}s_j$ is an effective transverse drive and $s_j = \langle \hat{\sigma}_x^{(j)} \rangle_{\text{mf}}$ is a mean-field approximation for spin j . The energy gap of spin i then increases with g as $\sqrt{\omega^2 + g^2\Omega_i^2}$ and interactions degrade performance.

Increasing the compression ratio increases performance until $r = r'$, with $r' \sim 1.1$ at $g = g_c(p)$, at which point the performance abruptly drops, see Fig. 1(c). Unlike the non-interacting case, the peak work output and efficiency can both occur at a comparable compression ratio. Equation (4) describes this behaviour: within this approximation, performance increases until $1 - \Delta_2/\Delta_1 \sim \eta_C$, with $\eta_C = 1 - \beta_H/\beta_C$ the Carnot efficiency. Hence $r' \approx (1 - g\eta_C/g_c(p))/(1 - \eta_C) + O(g^2)$ diminishes with increasing g . As a result, for $g \sim g_c(p)$ we can have high efficiency at small compression ratios $r \sim r_{\text{NI}}^{\text{max}}$. Without interactions, the maximum compression ratio satisfies $1 - 1/r' = \eta_C$ and therefore $r' = 1/(1 - \eta_C) \gg r_{\text{NI}}^{\text{max}}$.

Effect of increasing temperature. As the temperature increases, thermal fluctuations render Eq. (4) invalid and we find that the performance enhancement relative to the non-interacting system is diminished, see Fig. 2(a). A performance enhancement is present as long as $\beta_H \gtrsim 4\omega_0^{-1}$ (the precise cross-over point is dependent on g), coinciding with the regime where only the ground and first N excited levels are appreciably occupied, see Fig. 2(b). The transverse Ising model gives a qualitative understanding of this diminished performance enhancement. The first N excited energy levels of this model are $\sqrt{\omega^2 + g^2 - 2\omega g \cos \theta_k}$ with $\theta_k = 2\pi k/N$ ($k = 0, \dots, N-1$) [71]. Interactions diminish the energy of only the lowest $N/2$ excited levels, with the most pronounced reduction occurring for the first excited level ($k = 0$). Hence, the enhancement is largest when only the first excited level is occupied, and diminishes as more excited levels are occupied. The efficiency enhancement is most robust to increasing temperature for long-range interactions, see Fig. 2(a,ii). At a given temperature, the occupation $\sum_{i=2}^N n_i$ decreases as the range of interactions increases, see Fig. 2(b). Hence long-range interactions are most effective at suppressing fluctuations beyond the

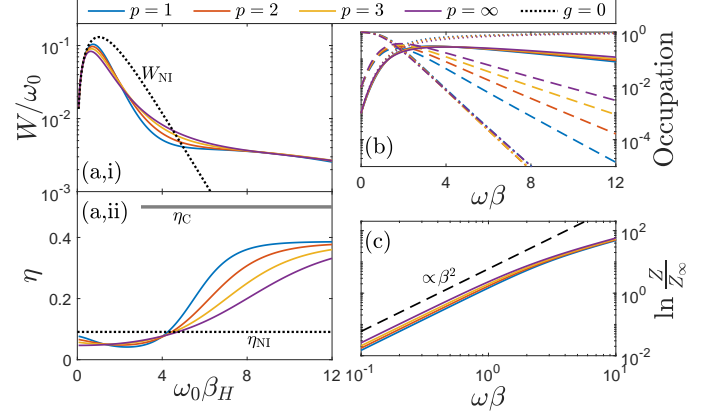


FIG. 2. (a) Adiabatic engine performance for varying temperature ($r = 1.1$, $\beta_C = 2\beta_H$). (a,i) Work output and (a,ii) efficiency exceed the non-interacting values (dotted lines) for cold temperatures $\beta_H \gtrsim 4\omega_0^{-1}$, whereas interactions degrade performance for $\beta_H < 4\omega_0^{-1}$. The gray line in (a,ii) is the Carnot efficiency. (b) Thermal energy-level occupations n_0 (dotted lines), n_1 (solid lines), $\sum_{i=2}^N n_i$ (dashed lines) and $\sum_{i=N+1}^{2N-1} n_i$ (dash-dotted lines). Here $n_i = e^{-\beta E_i}/Z(\beta, \omega)$ is the thermal occupation of energy level i , indexed in order of increasing energy E_i . The performance enhancement occurs when occupation is predominantly in the ground and first N excited states. Long-range interactions suppress occupation beyond the first excited state, resulting in the highest efficiency in (a,ii). (c) Dimensionless free energy $\ln Z$ showing the β^2 scaling for $\beta \lesssim \omega^{-1}$, coinciding with the regime of low performance. All results are for a 10-spin chain at $g = g_c(p)$.

approximation (4). For $\beta_H < 4\omega_0^{-1}$, interactions degrade performance, see Fig. 2(a). Expanding the dimensionless free energy in powers of β , we obtain

$$\ln Z = \ln Z_\infty + \frac{\beta^2 \omega^2}{4} + \frac{\beta^2 g^2 \sum_i (\Omega'_i)^2}{4} + O(\beta^4), \quad (5)$$

with $Z_\infty = 2^N$ the infinite temperature partition function and $\Omega'_i = (1/2) \sum_{j \neq i} J_{ij}$ is Ω_i with $s_j = 1/2$. At order β^2 , the free energy is indistinguishable from the mean-field free energy $\sum_i \ln \text{Tr} e^{-\beta(\omega \hat{\sigma}_z^{(i)} - \Omega'_i \hat{\sigma}_x^{(i)})}$, in which case interactions degrade performance. The scaling $\ln(Z/Z_\infty) \propto \beta^2$ is clearly present for temperatures $\beta_H \lesssim \omega_0^{-1}$, see Fig. 2(c).

Diabatic work extraction. For diabatic (finite-time) work extraction, interactions generally degrade engine performance due to “quantum friction” [36, 37, 55]. This friction arises when the interaction component of the Hamiltonian does not commute with the driving component, and hence the density matrix develops off-diagonal elements in the energy eigenbasis. The diabatic performance of a $p = \infty$ engine with weak interactions is shown in Fig. 3(a). The peak power output occurs for a time step $\tau \approx 4\omega_0^{-1}$ (the precise value is dependent on g), at which point the efficiency is close to the adiabatic ef-

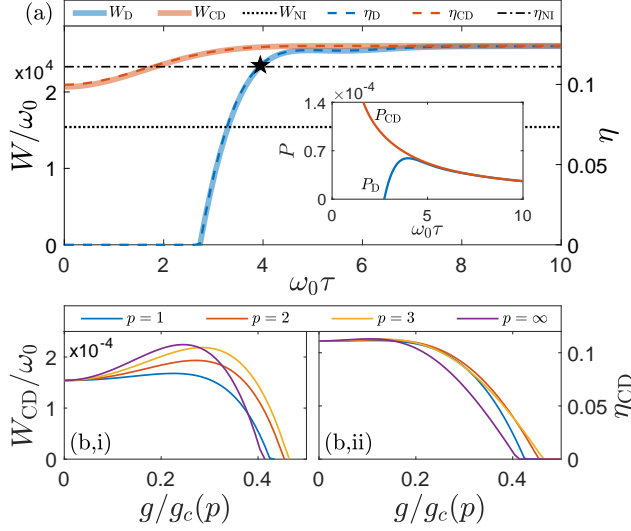


FIG. 3. (a) Diabatic work output W_D and efficiency η_D for $p = \infty$ with weak interactions $g/g_c = 0.2$. The maximum power output P_D (see inset) occurs at $\tau \approx 4\omega_0^{-1}$ (star), with performance rapidly declining for smaller τ . The approximate counterdiabatic driving (Eq. (6)) results in work output (W_{CD}) and efficiency (η_{CD}) close to the adiabatic performance even for rapid engine cycles. The counterdiabatic power output (P_{CD}) grows as τ^{-1} (inset). (b) The effectiveness of Eq. (6) diminishes for larger $g/g_c(p)$ or smaller p (results for $\tau = \omega_0^{-1}$; for $p = \infty$, we use the exact χ_{ij} , whereas for $p = 1, 2, 3$, we set $\chi_{ij} = 1$). All results are for $N = 10$ and $r = r_{NI}^{\max}$.

efficiency. For faster cycles, the performance rapidly decreases.

In principle, quantum friction can be mitigated completely using a counterdiabatic driving field \hat{H}_{cd} [77, 78]. In practice, exact counterdiabatic driving in a many-body system requires unrealistic interactions between all particles [79–85], and approximate protocols are required. A powerful approximation method is to find \hat{H}_{cd} variationally by minimising the action $S = \text{Tr}[G(\hat{H}_{cd})^2]$, with $G(\hat{H}_{cd}) = \partial\hat{H}/\partial t + i[\hat{H}_{cd}, \hat{H}]$ and \hat{H}_{cd} expanded in some truncated set of operators [86, 87]. We use $\hat{H}_{cd} = \sum_{ij(j \neq i)} C_{ij} \hat{\sigma}_x^{(i)} \hat{\sigma}_y^{(j)}$, which is the optimal counterdiabatic drive over all one-body and two-body operators [68] (c.f. [88]). For large N in the paramagnetic phase, we obtain [68],

$$\hat{H}_{cd} = - \sum_{\substack{i,j=1 \\ (j \neq i)}}^N \frac{g\omega'(t)J_{ij}}{2\omega(t)^2} \chi_{ij}(t) \hat{\sigma}_x^{(i)} \hat{\sigma}_y^{(j)}, \quad (6)$$

with $\chi_{ij}(t) = 1 + O(g^2/\omega^2)$ given in [68]. The work protocols $f(t)$ and $f(\tau - t)$ satisfy $f'(0) = f'(\tau) = 0$, and hence the net power transferred to the counterdiabatic drive field is zero [89].

For nearest neighbour interactions, $\chi_{ij} = 1/(1 + g^2/\omega(t)^2)$ and Eq. (6) drastically improves the diabatic

engine operation for $g \lesssim 0.3g_c$, see Fig. 3. For rapid cycles, the work output approaches a constant with little cost in efficiency, and hence the power P increases as τ^{-1} . In practice, the time scale of the thermalization steps will limit the engine to finite power [26, 90]. Note $\eta \propto W$ irrespective of counterdiabatic driving (Fig. 3(a)), hence Q_H depends only weakly on τ .

For increasing g/g_c there is a trade-off in the performance gained from interactions and the performance lost from quantum friction, with peak performance occurring for $g/g_c \approx 0.3$ for $\tau = \omega_0^{-1}$. Here, the work output from a chain with nearest neighbour interactions is about 50% larger than the non-interacting chain and both show comparable efficiency, see Fig. 3(b). For $p = 1, 2, 3$, $\chi_{ij}(t)$ is difficult to engineer since the interactions must be re-configured at different times. To simplify, we expand to lowest order in g/ω and set $\chi_{ij}(t) = 1$. While this is somewhat effective at mitigating diabatic degradation for weak interactions, the performance enhancement diminishes as the range of interactions increases. Hence a chain with $p = 1$, $g/g_c \lesssim 0.3$ and $\tau = \omega_0^{-1}$ has approximately the same performance as a non-interacting chain. Interestingly, we find that Eq. (6) is most effective for $\beta_H \lesssim 10\omega_0^{-1}$, with reduced performance for colder temperatures. This may be due to thermal fluctuations countering quantum friction [91].

Conclusion. We have shown that an engine of interacting spins outperforms a non-interacting engine in the paramagnetic phase for low temperatures and adiabatic operation, due to a lowering of the first excited state energy gap. The enhancement in work output is particular pronounced, with W/W_{NI} increasing exponentially with increasing interactions. The efficiency enhancement is largest for long-range interactions, which suppress occupation of energy levels beyond the first excited state. A performance enhancement due to long-range interactions has also been identified in Kitaev chains [92, 93]. For diabatic engine operation, quantum friction degrades performance. We have presented one counterdiabatic method that mitigates friction for weak interactions, however other methods could be explored [79, 85, 91, 94–99]. Modulating the phase and detuning of the drive profile may better isolate the two lowest energy eigenstates [100–104], limiting degradation due to thermal fluctuations and quantum friction. The low-temperature performance enhancement is a many-body quantum effect due to bipartite entanglement arising from the first excited state. A more thorough investigation of the entanglement properties of the thermal spin chain could reveal how entanglement changes for higher temperatures [105–108] or diabatic operation.

Acknowledgements. We thank C. Woffinden and M. Edmonds for useful comments on the manuscript. This research was supported by the Australian Research Council Centre of Excellence for Engineered Quantum Systems (EQUS, CE170100009).

-
- [1] J. Millen and A. Xuereb, Perspective on quantum thermodynamics, *New J. Phys.* **18**, 011002 (2016).
 - [2] M. O. Scully, M. S. Zubairy, G. S. Agarwal, and H. Walther, Extracting work from a single heat bath via vanishing quantum coherence, *Science* **299**, 862 (2003).
 - [3] A. Ü. C. Hardal and Ö. E. Müstecaplıoğlu, Superradiant quantum heat engine, *Sci. Rep.* **5**, 12953 (2015).
 - [4] K. Hammam, H. Leitch, Y. Hassouni, and G. De Chiara, Exploiting coherence for quantum thermodynamic advantage, *New J. Phys.* **24**, 113053 (2022).
 - [5] X. L. Huang, T. Wang, and X. X. Yi, Effects of reservoir squeezing on quantum systems and work extraction, *Phys. Rev. E* **86**, 051105 (2012).
 - [6] J. Roßnagel, O. Abah, F. Schmidt-Kaler, K. Singer, and E. Lutz, Nanoscale heat engine beyond the Carnot limit, *Phys. Rev. Lett.* **112**, 030602 (2014).
 - [7] G. Manzano, F. Galve, R. Zambrini, and J. M. R. Parrondo, Entropy production and thermodynamic power of the squeezed thermal reservoir, *Phys. Rev. E* **93**, 052120 (2016).
 - [8] W. Niedenzu, D. Gelbwaser-Klimovsky, A. G. Kofman, and G. Kurizki, On the operation of machines powered by quantum non-thermal baths, *New J. Phys.* **18**, 083012 (2016).
 - [9] J. Klaers, S. Faelt, A. Imamoglu, and E. Togan, Squeezed thermal reservoirs as a resource for a nanomechanical engine beyond the Carnot limit, *Phys. Rev. X* **7**, 031044 (2017).
 - [10] B. K. Agarwalla, J.-H. Jiang, and D. Segal, Quantum efficiency bound for continuous heat engines coupled to noncanonical reservoirs, *Phys. Rev. B* **96**, 104304 (2017).
 - [11] W. Niedenzu, V. Mukherjee, A. Ghosh, A. G. Kofman, and G. Kurizki, Quantum engine efficiency bound beyond the second law of thermodynamics, *Nat. Commun.* **9**, 165 (2018).
 - [12] R. Dillenschneider and E. Lutz, Energetics of quantum correlations, *EPL* **88**, 50003 (2009).
 - [13] O. Abah and E. Lutz, Efficiency of heat engines coupled to nonequilibrium reservoirs, *EPL* **106**, 20001 (2014).
 - [14] P. Kammerlander and J. Anders, Coherence and measurement in quantum thermodynamics, *Sci. Rep.* **6**, 22174 (2016).
 - [15] K. Korzekwa, M. Lostaglio, J. Oppenheim, and D. Jennings, The extraction of work from quantum coherence, *New J. Phys.* **18**, 023045 (2016).
 - [16] R. Uzdin, Coherence-induced reversibility and collective operation of quantum heat machines via coherence recycling, *Phys. Rev. Appl.* **6**, 024004 (2016).
 - [17] H. Tajima and K. Funo, Superconducting-like heat current: Effective cancellation of current-dissipation trade-off by quantum coherence, *Phys. Rev. Lett.* **127**, 190604 (2021).
 - [18] R. Uzdin, A. Levy, and R. Kosloff, Equivalence of quantum heat machines, and quantum-thermodynamic signatures, *Phys. Rev. X* **5**, 031044 (2015).
 - [19] J. Klatzow, J. N. Becker, P. M. Ledingham, C. Weinzetl, K. T. Kaczmarek, D. J. Saunders, J. Nunn, I. A. Walmsey, R. Uzdin, and E. Poem, Experimental demonstration of quantum effects in the operation of microscopic heat engines, *Phys. Rev. Lett.* **122**, 110601 (2019).
 - [20] J. Jaramillo, B. M., and A. del Campo, Quantum supremacy of many-particle thermal machines, *New J. Phys.* **18**, 075019 (2016).
 - [21] J. Bengtsson, M. N. Tengstrand, A. Wacker, P. Samuelsson, M. Ueda, H. Linke, and S. M. Reimann, Quantum Szilard engine with attractively interacting bosons, *Phys. Rev. Lett.* **120**, 100601 (2018).
 - [22] T. Fogarty and T. Busch, A many-body heat engine at criticality, *Quantum Sci. Technol.* **6**, 015003 (2020).
 - [23] M. Boubakour, T. Fogarty, and T. Busch, Interaction enhanced quantum heat engine, arXiv:2211.03394 (2022).
 - [24] Y.-Y. Chen, G. Watanabe, Y.-C. Yu, X.-W. Guan, and A. del Campo, An interaction-driven many-particle quantum heat engine and its universal behavior, *npj Quantum Inf.* **5**, 88 (2019).
 - [25] F. Carollo, F. M. Gambetta, K. Brandner, J. P. Garrahan, and I. Lesanovsky, Nonequilibrium quantum many-body Rydberg atom engine, *Phys. Rev. Lett.* **124**, 170602 (2020).
 - [26] E. Geva and R. Kosloff, A quantum-mechanical heat engine operating in finite time. A model consisting of spin-1/2 systems as the working fluid, *J. Chem. Phys.* **96**, 3054 (1992).
 - [27] D. von Lindenfels, O. Gräb, C. T. Schmiegelow, V. Kaushal, J. Schulz, M. T. Mitchison, J. Goold, F. Schmidt-Kaler, and U. G. Poschinger, Spin heat engine coupled to a harmonic-oscillator flywheel, *Phys. Rev. Lett.* **123**, 080602 (2019).
 - [28] J. P. S. Peterson, T. B. Batalhão, M. Herrera, A. M. Souza, R. S. Sarthour, I. S. Oliveira, and R. M. Serra, Experimental characterization of a spin quantum heat engine, *Phys. Rev. Lett.* **123**, 240601 (2019).
 - [29] W. Niedenzu and G. Kurizki, Cooperative many-body enhancement of quantum thermal machine power, *New J. Phys.* **20**, 113038 (2018).
 - [30] M. Kloc, P. Cejnar, and G. Schaller, Collective performance of a finite-time quantum Otto cycle, *Phys. Rev. E* **100**, 042126 (2019).
 - [31] K. Ono, S. N. Shevchenko, T. Mori, S. Moriyama, and F. Nori, Analog of a quantum heat engine using a single-spin qubit, *Phys. Rev. Lett.* **125**, 166802 (2020).
 - [32] J. Wang, Z. Wu, and J. He, Quantum Otto engine of a two-level atom with single-mode fields, *Phys. Rev. E* **85**, 041148 (2012).
 - [33] R. Wang, J. Wang, J. He, and Y. Ma, Efficiency at maximum power of a heat engine working with a two-level atomic system, *Phys. Rev. E* **87**, 042119 (2013).
 - [34] T. D. Kieu, The second law, Maxwell's demon, and work derivable from quantum heat engines, *Phys. Rev. Lett.* **93**, 140403 (2004).
 - [35] W. Ji, Z. Chai, M. Wang, Y. Guo, X. Rong, F. Shi, C. Ren, Y. Wang, and J. Du, Spin quantum heat engine quantified by quantum steering, *Phys. Rev. Lett.* **128**, 090602 (2022).
 - [36] R. Kosloff and T. Feldmann, Discrete four-stroke quantum heat engine exploring the origin of friction, *Phys. Rev. E* **65**, 055102 (2002).
 - [37] T. Feldmann and R. Kosloff, Quantum four-stroke heat engine: Thermodynamic observables in a model with intrinsic friction, *Phys. Rev. E* **68**, 016101 (2003).
 - [38] T. Feldmann and R. Kosloff, Characteristics of the limit cycle of a reciprocating quantum heat engine, *Phys. Rev. E* **70**, 046110 (2004).

- [39] T. Zhang, W.-T. Liu, P.-X. Chen, and C.-Z. Li, Four-level entangled quantum heat engines, *Phys. Rev. A* **75**, 062102 (2007).
- [40] G. Zhang, Entangled quantum heat engines based on two two-spin systems with Dzyaloshinski-Moriya anisotropic antisymmetric interaction, *Eur. Phys. J. D* **49**, 123 (2008).
- [41] H. Wang, S. Liu, and J. He, Thermal entanglement in two-atom cavity QED and the entangled quantum Otto engine, *Phys. Rev. E* **79**, 041113 (2009).
- [42] G. Thomas and R. S. Johal, Coupled quantum Otto cycle, *Phys. Rev. E* **83**, 031135 (2011).
- [43] F. Altintas and O. E. Müstecaplıoğlu, General formalism of local thermodynamics with an example: Quantum Otto engine with a spin-1/2 coupled to an arbitrary spin, *Phys. Rev. E* **92**, 022142 (2015).
- [44] L.-M. Zhao and G.-F. Zhang, Entangled quantum Otto heat engines based on two-spin systems with the Dzyaloshinski-Moriya interaction, *Quant. Inf. Process.* **16**, 216 (2017).
- [45] S. Çakmak, F. Altintas, and Ö. E. Müstecaplıoğlu, Lipkin-Meshkov-Glick model in a quantum Otto cycle, *The European Physical Journal Plus* **131**, 197 (2016).
- [46] A. Hewgill, A. Ferraro, and G. De Chiara, Quantum correlations and thermodynamic performances of two-qubit engines with local and common baths, *Phys. Rev. A* **98**, 042102 (2018).
- [47] S. Chand and A. Biswas, Critical-point behavior of a measurement-based quantum heat engine, *Phys. Rev. E* **98**, 052147 (2018).
- [48] G. Piccitto, M. Campisi, and D. Rossini, The Ising critical quantum Otto engine, *New J. Phys.* **24**, 103023 (2022).
- [49] B. S. Revathy, V. Mukherjee, U. Divakaran, and A. del Campo, Universal finite-time thermodynamics of many-body quantum machines from Kibble-Zurek scaling, *Phys. Rev. Research* **2**, 043247 (2020).
- [50] D. Porras and J. I. Cirac, Effective quantum spin systems with trapped ions, *Phys. Rev. Lett.* **92**, 207901 (2004).
- [51] J. W. Britton, B. C. Sawyer, A. C. Keith, C.-C. J. Wang, J. K. Freericks, H. Uys, M. J. Biercuk, and J. J. Bollinger, Engineered two-dimensional Ising interactions in a trapped-ion quantum simulator with hundreds of spins, *Nature* **484**, 489 (2012).
- [52] J. G. Bohnet, B. C. Sawyer, J. W. Britton, M. L. Wall, A. M. Rey, M. Foss-Feig, and J. J. Bollinger, Quantum spin dynamics and entanglement generation with hundreds of trapped ions, *Science* **352**, 1297 (2016).
- [53] J. Zhang, G. Pagano, P. W. Hess, A. Kyprianidis, P. Becker, H. Kaplan, A. V. Gorshkov, Z.-X. Gong, and C. Monroe, Observation of a many-body dynamical phase transition with a 53-qubit quantum simulator, *Nature* **551**, 601 (2017).
- [54] C. Monroe, W. C. Campbell, L.-M. Duan, Z.-X. Gong, A. V. Gorshkov, P. W. Hess, R. Islam, K. Kim, N. M. Linke, G. Pagano, P. Richerme, C. Senko, and N. Y. Yao, Programmable quantum simulations of spin systems with trapped ions, *Rev. Mod. Phys.* **93**, 025001 (2021).
- [55] F. Plastina, A. Alecce, T. J. G. Apollaro, G. Falcone, G. Francica, F. Galve, N. Lo Gullo, and R. Zambrini, Irreversible work and inner friction in quantum thermodynamic processes, *Phys. Rev. Lett.* **113**, 260601 (2014).
- [56] A. Dutta and J. K. Bhattacharjee, Phase transitions in the quantum Ising and rotor models with a long-range interaction, *Phys. Rev. B* **64**, 184106 (2001).
- [57] S. Fey and K. P. Schmidt, Critical behavior of quantum magnets with long-range interactions in the thermodynamic limit, *Phys. Rev. B* **94**, 075156 (2016).
- [58] N. Defenu, A. Trombettoni, and S. Ruffo, Criticality and phase diagram of quantum long-range $O(N)$ models, *Phys. Rev. B* **96**, 104432 (2017).
- [59] L. Vanderstraeten, M. Van Damme, H. P. Büchler, and F. Verstraete, Quasiparticles in quantum spin chains with long-range interactions, *Phys. Rev. Lett.* **121**, 090603 (2018).
- [60] Z. Zhu, G. Sun, W.-L. You, and D.-N. Shi, Fidelity and criticality of a quantum Ising chain with long-range interactions, *Phys. Rev. A* **98**, 023607 (2018).
- [61] E. Gonzalez-Lazo, M. Heyl, M. Dalmonte, and A. Angelone, Finite-temperature critical behavior of long-range quantum Ising models, *SciPost Phys.* **11**, 76 (2021).
- [62] J. A. Koziol, A. Langheld, S. C. Kapfer, and K. P. Schmidt, Quantum-critical properties of the long-range transverse-field Ising model from quantum Monte Carlo simulations, *Phys. Rev. B* **103**, 245135 (2021).
- [63] In analogy with the ideal gas Otto cycle, where the compression ratio is given by the ratio of maximum and minimum gas volumes.
- [64] M. Born and V. Fock, Beweis des adiabatensatzes, *Zeitschrift für Physik* **51**, 165 (1928).
- [65] T. Kato, On the adiabatic theorem of quantum mechanics, *J. Phys. Soc. Jpn.* **5**, 435 (1950).
- [66] J. E. Avron and A. Elgart, Adiabatic theorem without a gap condition, *Comm. Math. Phys.* **203**, 445 (1999).
- [67] D. J. Griffiths and D. F. Schroeter, *Introduction to Quantum Mechanics*, 3rd ed. (Cambridge University Press, Cambridge, 2018).
- [68] See Supplemental Material at [URL will be inserted by publisher] for calculation of $g_c(p)$, system-size scaling, and analytic calculations, which includes Refs. [109–115].
- [69] A. Campa, T. Dauxois, and S. Ruffo, Statistical mechanics and dynamics of solvable models with long-range interactions, *Phys. Rep.* **480**, 57 (2009).
- [70] N. Defenu, T. Donner, T. Macrì, G. Pagano, S. Ruffo, and A. Trombettoni, Long-range interacting quantum systems, arXiv:2109.01063 (2021).
- [71] P. Pfeuty, The one-dimensional Ising model with a transverse field, *Ann. Phys.* **57**, 79 (1970).
- [72] In a frame where ground-state energy is zero. The dimensionless free energy is the free energy divided by $k_B T$.
- [73] T. Holstein and H. Primakoff, Field dependence of the intrinsic domain magnetization of a ferromagnet, *Phys. Rev.* **58**, 1098 (1940).
- [74] A. Peres, Separability criterion for density matrices, *Phys. Rev. Lett.* **77**, 1413 (1996).
- [75] M. Horodecki, P. Horodecki, and R. Horodecki, Separability of mixed states: necessary and sufficient conditions, *Phys. Lett. A* **223**, 1 (1996).
- [76] G. Tóth and O. Gühne, Entanglement and permutational symmetry, *Phys. Rev. Lett.* **102**, 170503 (2009).
- [77] M. Demirplak and S. A. Rice, Adiabatic population transfer with control fields, *J. Phys. Chem. A* **107**, 9937

- (2003).
- [78] M. V. Berry, Transitionless quantum driving, *J. Phys. A: Math. Theor.* **42**, 365303 (2009).
 - [79] A. del Campo, M. M. Rams, and W. H. Zurek, Assisted finite-rate adiabatic passage across a quantum critical point: Exact solution for the quantum Ising model, *Phys. Rev. Lett.* **109**, 115703 (2012).
 - [80] A. del Campo, Shortcuts to adiabaticity by counterdiabatic driving, *Phys. Rev. Lett.* **111**, 100502 (2013).
 - [81] S. Deffner, C. Jarzynski, and A. del Campo, Classical and quantum shortcuts to adiabaticity for scale-invariant driving, *Phys. Rev. X* **4**, 021013 (2014).
 - [82] H. Saberi, T. Opatrny, K. Mølmer, and A. del Campo, Adiabatic tracking of quantum many-body dynamics, *Phys. Rev. A* **90**, 060301 (2014).
 - [83] S. Campbell, G. De Chiara, M. Paternostro, G. M. Palma, and R. Fazio, Shortcut to adiabaticity in the Lipkin-Meshkov-Glick model, *Phys. Rev. Lett.* **114**, 177206 (2015).
 - [84] G. Passarelli, V. Cataudella, R. Fazio, and P. Lucignano, Counterdiabatic driving in the quantum annealing of the p -spin model: A variational approach, *Phys. Rev. Research* **2**, 013283 (2020).
 - [85] I. Čepaitė, A. Polkovnikov, A. J. Daley, and C. W. Duncan, Counterdiabatic optimized local driving, *PRX Quantum* **4**, 010312 (2023).
 - [86] D. Sels and A. Polkovnikov, Minimizing irreversible losses in quantum systems by local counterdiabatic driving, *Proc. Natl. Acad. Sci. U.S.A.* **114**, E3909 (2017).
 - [87] M. Kolodrubetz, D. Sels, P. Mehta, and A. Polkovnikov, Geometry and non-adiabatic response in quantum and classical systems, *Phys. Rep.* **697**, 1 (2017).
 - [88] A. Hartmann, V. Mukherjee, W. Niedenzu, and W. Lechner, Many-body quantum heat engines with shortcuts to adiabaticity, *Phys. Rev. Research* **2**, 023145 (2020).
 - [89] This can be shown explicitly by integrating by parts the instantaneous power $\langle \partial(\hat{H} + \hat{H}_{cd})/\partial t \rangle$ and noting that only the boundary term remains.
 - [90] F. L. Curzon and B. Ahlborn, Efficiency of a Carnot engine at maximum power output, *Am. J. Phys.* **43**, 22 (1975).
 - [91] T. Feldmann and R. Kosloff, Quantum lubrication: Suppression of friction in a first-principles four-stroke heat engine, *Phys. Rev. E* **73**, 025107 (2006).
 - [92] Q. Wang, Performance of quantum heat engines under the influence of long-range interactions, *Phys. Rev. E* **102**, 012138 (2020).
 - [93] A. Solfanelli, G. Giachetti, M. Campisi, S. Ruffo, and N. Defenu, Quantum heat engine with long-range advantages, arXiv:2208.09492 (2022).
 - [94] P. Sgroi, G. M. Palma, and M. Paternostro, Reinforcement learning approach to nonequilibrium quantum thermodynamics, *Phys. Rev. Lett.* **126**, 020601 (2021).
 - [95] A. Rolandi, M. Perarnau-Llobet, and H. J. Miller, Optimal control of dissipation and work fluctuations for rapidly driven systems, arXiv:2212.03927 (2022).
 - [96] S. Deffner and M. V. S. Bonança, Thermodynamic control — An old paradigm with new applications, *EPL* **131**, 20001 (2020).
 - [97] V. Cavina, P. A. Erdman, P. Abiuso, L. Tolomeo, and V. Giovannetti, Maximum-power heat engines and refrigerators in the fast-driving regime, *Phys. Rev. A* **104**, 032226 (2021).
 - [98] A. Soriani, E. Miranda, S. Deffner, and M. V. S. Bonança, Shortcuts to thermodynamic quasistaticity, *Phys. Rev. Lett.* **129**, 170602 (2022).
 - [99] P. A. Erdman, A. Rolandi, P. Abiuso, M. Perarnau-Llobet, and F. Noé, Pareto-optimal cycles for power, efficiency and fluctuations of quantum heat engines using reinforcement learning, arXiv:2207.13104 (2022).
 - [100] G. Facchinetti, S. D. Jenkins, and J. Ruostekoski, Storing light with subradiant correlations in arrays of atoms, *Phys. Rev. Lett.* **117**, 243601 (2016).
 - [101] G. Facchinetti and J. Ruostekoski, Interaction of light with planar lattices of atoms: Reflection, transmission, and cooperative magnetometry, *Phys. Rev. A* **97**, 023833 (2018).
 - [102] L. A. Williamson and J. Ruostekoski, Optical response of atom chains beyond the limit of low light intensity: The validity of the linear classical oscillator model, *Phys. Rev. Research* **2**, 023273 (2020).
 - [103] L. A. Williamson, M. O. Borgh, and J. Ruostekoski, Supercritical picture of collective nonclassical light emission and dipole blockade in atom arrays, *Phys. Rev. Lett.* **125**, 073602 (2020).
 - [104] A. Cidrim, T. S. do Espirito Santo, J. Schachenmayer, R. Kaiser, and R. Bachelard, Photon blockade with ground-state neutral atoms, *Phys. Rev. Lett.* **125**, 073601 (2020).
 - [105] D. Gunlycke, V. M. Kendon, V. Vedral, and S. Bose, Thermal concurrence mixing in a one-dimensional Ising model, *Phys. Rev. A* **64**, 042302 (2001).
 - [106] T. J. Osborne and M. A. Nielsen, Entanglement in a simple quantum phase transition, *Phys. Rev. A* **66**, 032110 (2002).
 - [107] B. V. Fine, F. Mintert, and A. Buchleitner, Equilibrium entanglement vanishes at finite temperature, *Phys. Rev. B* **71**, 153105 (2005).
 - [108] T. Yu and J. H. Eberly, Sudden death of entanglement, *Science* **323**, 598 (2009).
 - [109] M. Kac, G. E. Uhlenbeck, and P. C. Hemmer, On the van der Waals theory of the vapor-liquid equilibrium. I. Discussion of a one-dimensional model, *J. Math. Phys.* **4**, 216 (1963).
 - [110] M. Kac and C. J. Thompson, Critical behavior of several lattice models with long-range interaction, *J. Math. Phys.* **10**, 1373 (1969).
 - [111] S. A. Cannas and F. A. Tamarit, Long-range interactions and nonextensivity in ferromagnetic spin models, *Phys. Rev. B* **54**, R12661 (1996).
 - [112] M. Vogl, P. Laurell, H. Zhang, S. Okamoto, and G. A. Fiete, Resummation of the Holstein-Primakoff expansion and differential equation approach to operator square roots, *Phys. Rev. Research* **2**, 043243 (2020).
 - [113] J. König and A. Hucht, Newton series expansion of bosonic operator functions, *SciPost Phys.* **10**, 007 (2021).
 - [114] L. Cevolani, G. Carleo, and L. Sanchez-Palencia, Spreading of correlations in exactly solvable quantum models with long-range interactions in arbitrary dimensions, *New J. Phys.* **18**, 093002 (2016).
 - [115] J. Wu, X. Zhang, and D. Liu, An efficient calculation of the Clausen functions $Cl_n(\theta)$ ($n \geq 2$), *BIT Numer. Math.* **50**, 193 (2010).

Supplemental Material to “Many-body enhancement in a spin-chain quantum heat engine”

L. A. Williamson¹ and Matthew J. Davis¹

¹*ARC Centre of Excellence for Engineered Quantum Systems, School of Mathematics and Physics,
University of Queensland, St Lucia, Queensland 4072, Australia*

(Dated: February 6, 2023)

In this supplemental material we show how $g_c(p)$ is determined from the energy gap of the system, we show how the engine performance scales with system size, and derive expressions for the analytic dimensionless free energy, the entanglement entropy, and the counterdiabatic driving.

S.A. Energy gap, critical point and scaling with system size

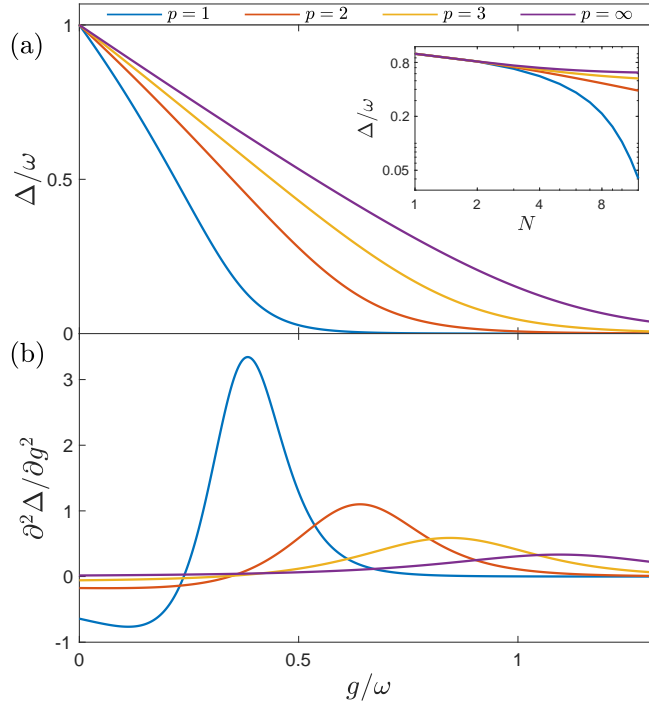


FIG. S1. (a) Energy gap Δ between ground and first excited state for a 10-spin chain. The energy gap decreases as $\Delta = 1 - g/g_c(p) + O(g^2)$, where $g_c(p)$ is the critical interaction strength separating the paramagnetic and ferromagnetic phases. In the finite-sized system, we define $g_c(p)$ to be the point where $\partial^2\Delta/\partial g^2$, shown in (b), is a maximum. Inset in (a) shows the dependence of Δ on N for $g = 0.4\omega$.

The energy gap Δ between the ground and first excited state is shown in Fig. S1(a). The energy gap decreases approximately linearly with increasing $g/g_c(p)$. In an infinite system with nearest neighbour interactions, the exact energy gap is $\Delta = |\omega - g|$ [S1] and hence $\partial^2\Delta/\partial g^2 = \delta(\omega - g)$. Finite-size effects regularize the divergence of $\partial^2\Delta/\partial g^2$, however we still observe a clear peak at a critical value of g , see Fig. S1(b). We define $g_c(p)$ to be the value of g corresponding to this peak. The critical value is close to ω for $p = \infty$ and decreases for decreasing p . The critical value will depend on ω . In the main text, we fix $g_c(p)$ by defining this to be the critical value at $\omega = \omega_0$.

The dependence of work and efficiency on chain size N is shown in Fig. S2(a) for $g = 0.4\omega_0$. For $p = \infty, 3$ the performance scales extensively for $N \gtrsim 6$. Finite size effects are slightly more pronounced for $p = 2$, however the scaling is close to extensive. For $p = 1$ the performance scales super-extensively with g . This is due to a dependence of Δ on N , see inset to Fig. S1(a). The critical point g_c also depends on N for $p = 1$. In the cold, perturbative limit

(see next section), $\Delta \sim \omega - g(\gamma + \ln N)$ with γ the Euler-Mascheroni constant. The two-level approximation [Eq. 4 in the main text] then gives $W \sim N^{1+\beta_H g}$. This approximation captures the dependence of work on particle number for small g/g_c , see Fig. S2(a,ii),(b,ii). Increasing either g or N increases g/g_c and the perturbative approximation $W \sim N^{1+\beta_H g}$ breaks down. Scaling g by g_c effectively Kac renormalizes the interactions, rendering the long-range system extensive [S2–S6].

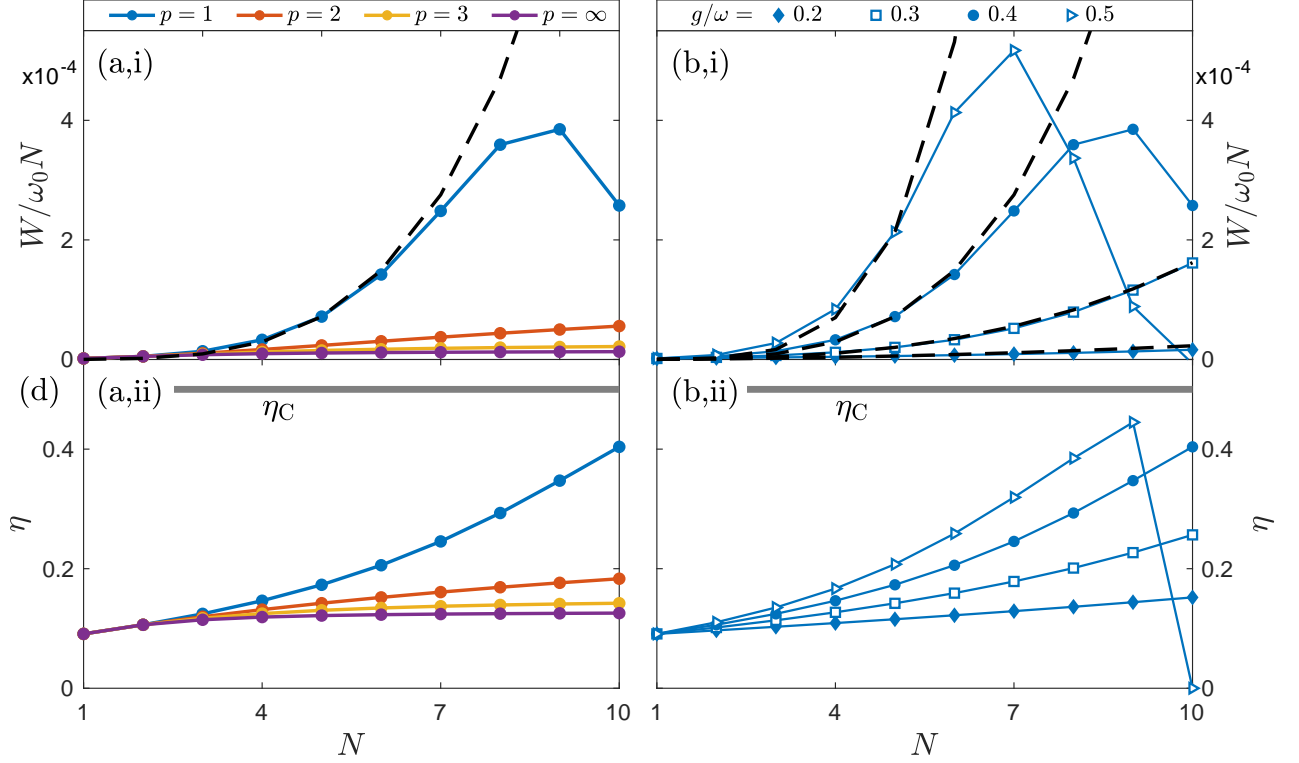


FIG. S2. The (a,i) work output and (a,ii) efficiency scale approximately extensively for $p = 2, 3, \infty$ whereas they scale non-extensively for $p = 1$. The non-extensive scaling for $p = 1$ agrees with the perturbative prediction $W \sim N^{1+\beta_H g}$ (black dashed lines). Results for $g = 0.4\omega_0$. (b) The non-extensive scaling of W and η for $p = 1$ and $g/\omega_0 = 0.2, 0.3, 0.4, 0.5$ along with the perturbative prediction $W \sim N^{1+\beta_H g}$ (matching dashed black lines). The gray lines in (a,ii),(b,ii) are the Carnot efficiency η_C . All results are for $\beta_H = 10\omega_0^{-1}$, $\beta_C = 2\beta_H$ and $r = r_{\text{NI}}^{\text{max}}$.

S.B. Performance of the transverse Ising model

The dimensionless free energy (free energy divided by $k_B T$) of the transverse Ising model confined to the first N excited states is

$$\begin{aligned} \ln Z &= \sum_{k=0}^{N-1} e^{-\beta \sqrt{\omega^2 + g^2 - 2\omega g \cos(2\pi k/N)}}, \\ &\approx \frac{N}{\pi} \int_0^\pi e^{-\beta \sqrt{\omega^2 + g^2 - 2\omega g \cos \theta}} d\theta. \end{aligned} \quad (\text{S1})$$

Here and below we work in a frame where the ground state energy is zero. In the adiabatic limit, the system energy at the four points in the cycle in Fig. 1(a) of the main text are

$$\begin{aligned}
(1) \quad \langle E \rangle &= \frac{N}{\pi} \int_0^\pi \sqrt{r^2 \omega_0^2 + g^2 - 2r\omega_0 g \cos \theta} e^{-\beta_H \sqrt{r^2 \omega_0^2 + g^2 - 2r\omega_0 g \cos \theta}} d\theta, \\
(2) \quad \langle E \rangle &= \frac{N}{\pi} \int_0^\pi \sqrt{\omega_0^2 + g^2 - 2\omega_0 g \cos \theta} e^{-\beta_H \sqrt{\omega_0^2 + g^2 - 2\omega_0 g \cos \theta}} d\theta, \\
(3) \quad \langle E \rangle &= \frac{N}{\pi} \int_0^\pi \sqrt{\omega_0^2 + g^2 - 2\omega_0 g \cos \theta} e^{-\beta_C \sqrt{\omega_0^2 + g^2 - 2\omega_0 g \cos \theta}} d\theta, \\
(4) \quad \langle E \rangle &= \frac{N}{\pi} \int_0^\pi \sqrt{r^2 \omega_0^2 + g^2 - 2r\omega_0 g \cos \theta} e^{-\beta_C \sqrt{\omega_0^2 + g^2 - 2\omega_0 g \cos \theta}} d\theta.
\end{aligned} \tag{S2}$$

The heat and work outputs can be computed from these, see Fig. 1(b) in the main text.

S.C. Perturbative treatment

We assume a large chain so that boundary effects can be ignored and hence we approximate the system as being translationally invariant (equivalently we can impose periodic boundary conditions). The spin operators can be converted to expressions in terms of bosonic operators via a Holstein-Primakoff transformation [S7],

$$\hat{\sigma}_x^{(i)} \rightarrow \frac{\left(\sqrt{1 - \hat{a}_i^\dagger \hat{a}_i}\right) \hat{a}_i + \hat{a}_i^\dagger \left(\sqrt{1 - \hat{a}_i^\dagger \hat{a}_i}\right)}{2}, \quad \hat{\sigma}_z^{(i)} \rightarrow \frac{1}{2} - \hat{a}_i^\dagger \hat{a}_i. \tag{S3}$$

In the low excitation regime we expand the Hamiltonian [Eq. 1 in the main text] to quadratic order in the bosonic operators $\hat{a}_i, \hat{a}_i^\dagger$. This gives [S7–S9]

$$\hat{H} = -\frac{\omega N}{2} + \omega \sum_{i=1}^N \hat{a}_i^\dagger \hat{a}_i - \frac{g}{4} \sum_{\substack{i,j=1 \\ (j \neq i)}}^N J_{ij} \left(\hat{a}_i + \hat{a}_i^\dagger \right) \left(\hat{a}_j + \hat{a}_j^\dagger \right). \tag{S4}$$

Fourier transforming and carrying out a Bogoliubov transformation gives [S10]

$$\hat{H} = \epsilon_0 + \sum_{k=0}^{N-1} \left(\omega \operatorname{sign}(\omega - g\tilde{J}_k) \sqrt{1 - \frac{2g}{\omega} \tilde{J}_k} \right) b_k^\dagger b_k, \tag{S5}$$

with ϵ_0 the ground-state energy, b_k bosonic operators for the quasiparticle modes and

$$\tilde{J}_k = \sum_{m=1}^N \frac{\cos(2\pi k m / N)}{m^p} = C_p^N \left(\frac{2\pi k}{N} \right), \tag{S6}$$

where $C_p^N(\theta) = \sum_{m=1}^N \cos(m\theta)/m^p$ is the finite- N generalized Clausen function [S11]. For nearest neighbour interactions, we have $\tilde{J}_k = \cos(2\pi k/N)$.

From hereon we assume $\operatorname{sign}(\omega - g\tilde{J}_k) > 0$. The thermodynamic properties of the spin chain can be determined from the partition function,

$$Z = \prod_{k=0}^{N-1} \frac{1}{1 - \exp\left(-\beta\omega\sqrt{1 - \frac{2g}{\omega}\tilde{J}_k}\right)}, \tag{S7}$$

with logarithm (dimensionless free energy),

$$\begin{aligned}
\ln Z &= \sum_{k=0}^{N-1} \ln \left[\frac{1}{1 - \exp\left(-\beta\omega\sqrt{1 - \frac{2g}{\omega}\tilde{J}_k}\right)} \right], \\
&\approx \sum_{k=0}^{N-1} \exp\left(-\beta\omega\sqrt{1 - \frac{2g}{\omega}\tilde{J}_k}\right).
\end{aligned} \tag{S8}$$

The latter approximation assumes low temperature. We have ignored the ground state energy, which adds an inconsequential constant to $\ln Z$. To proceed analytically, we presume small $g\tilde{J}_k/\omega$ and approximate $\sqrt{1 - 2g\tilde{J}_k/\omega} \approx 1 - g\tilde{J}_k/\omega$. Hence

$$\ln Z \approx e^{-\beta\omega} \sum_{k=0}^{N-1} \exp\left(m\beta g\tilde{J}_k\right). \quad (\text{S9})$$

We reserve a discussion of $p = 1$ for later and for now assume $p > 1$. For large N , $C_p^N(\theta) \rightarrow C_p(\theta) = \sum_{m=1}^{\infty} \cos(m\theta)/m^p$ and we can replace the sum over k in Eq. (S9) by an integral

$$\sum_{k=0}^{N-1} \exp\left(\beta g\tilde{J}_k\right) \rightarrow \frac{N}{\pi} \int_0^\pi \exp\left(\beta g C_p(\theta)\right) d\theta. \quad (\text{S10})$$

For even integers p ,

$$C_p(\theta) = -\frac{(-1)^{p/2}(2\pi)^p}{2p!} B_p\left(\frac{\theta}{2\pi}\right), \quad (\text{S11})$$

with $B_p(x)$ the Bernoulli polynomials, which are polynomials of order p . We obtain the following results for $p = \infty$ and $p = 2$,

$$\begin{aligned} \frac{1}{\pi} \int_0^\pi \exp(\beta g C_\infty(\theta)) d\theta &= \frac{1}{\pi} \int_0^\pi \exp(\beta g \cos(\theta)) d\theta = I_0(\beta g) \xrightarrow{\beta \rightarrow \infty} \frac{e^{\beta g}}{\sqrt{2\pi\beta g}}, \\ \frac{1}{\pi} \int_0^1 \exp(\beta g C_2(\theta)) d\theta &= \frac{2e^{\beta g \pi^2/6}}{\sqrt{\beta g \pi^2}} D\left(\frac{\sqrt{\beta g \pi^2}}{2}\right) \xrightarrow{\beta \rightarrow \infty} \frac{e^{\beta g \pi^2/6}}{3\beta g \pi^2/6}, \end{aligned} \quad (\text{S12})$$

where $I_0(x)$ is the modified Bessel function and $D(x)$ is Dawson's function (expressible in terms of the error function $\text{erf}(x)$ via $D(x) = -(\sqrt{\pi}/2)e^{-x^2}i \text{erf}(ix)$).

In general, for $p > 3$ the integral $\int_0^1 \exp((m\beta g C_p(2\pi x))) dx$ can be approximated at low temperatures using the method of steepest descent,

$$\frac{1}{\pi} \int_0^\pi \exp(\beta g C_p(\theta)) d\theta = \sqrt{\frac{1}{2\pi\beta g C_{p-2}(0)}} \exp(\beta g C_p(0)), \quad (\text{S13})$$

where $C_p(0) = \sum_{m=1}^{\infty} m^{-p} = \zeta(p)$. This does not work for $p = 2$ since $C_2'(\theta)|_{\theta=0} \neq 0$. This reflects that the spectrum is linear rather than quadratic around the lowest energy state. Nor does it work for $p = 3$, since $C_3''(\theta)|_{\theta=0}$ diverges. We observe numerically that $\exp(\beta g C_3(\theta))$ is dominated by its small θ behaviour for large βg . Hence for $p = 3$ we expand the Clausen function in a power series around the maximum $\theta = 0$,

$$\begin{aligned} \frac{1}{\pi} \int_0^\pi \exp(\beta g C_3(\theta)) d\theta &\approx \frac{\exp(\beta g \zeta(3))}{\pi} \int_0^\pi \exp\left(-\frac{\beta g \theta^2}{4} (3 - \ln \theta^2)\right) d\theta, \\ &= \frac{\exp(\beta g \zeta(3))}{\pi} \int_0^\pi \exp\left(-\frac{\beta g \theta^2}{4} (3 + \ln(\beta g) - \ln(\beta g \theta^2))\right) d\theta, \\ &= \frac{\exp(\beta g \zeta(3))}{\pi \sqrt{\beta g}} \int_0^{\pi \sqrt{\beta g}} u^{u^2/2} \exp\left(-\frac{1}{4} u^2 (\ln(\beta g) + 3)\right) du, \\ &\xrightarrow{\beta \rightarrow \infty} \frac{\exp(\beta g \zeta(3))}{\pi \sqrt{\beta g}} \int_0^{\pi \sqrt{\beta g}} \exp\left(-\frac{1}{4} u^2 (\ln(\beta g) + 3)\right) du, \\ &= \frac{\exp(\beta g \zeta(3))}{\sqrt{\pi \beta g (3 + \ln \beta g)}} \text{erf}\left(\frac{\pi}{2} \sqrt{3\beta g + \beta g \ln \beta g}\right), \\ &\xrightarrow{\beta \rightarrow \infty} \frac{\exp(\beta g \zeta(3))}{\sqrt{\pi \beta g (3 + \ln \beta g)}}. \end{aligned} \quad (\text{S14})$$

Hence we find a logarithmic correction $\ln \beta g$ to the partition function for $p = 3$, which interpolates between $p = 2$ and $p > 3$. Note that $3 > 2 \ln \pi \approx 2.29$ and so the expansion around $\theta = 0$ creates no convergence problems for

large $\theta > 1$. The asymptotic behaviour in the fourth line follows by replacing $u^{u^2/2}$ by $\lim_{u \rightarrow 0+} u^{u^2/2} = 1$ due to $\exp(-\frac{1}{4}u^2(\ln(\beta g) + 3))$ being sharply peaked around the origin for large βg . The validity of this approximation was confirmed numerically. Equations (S12) and (S14) give $\ln Z = N\mathcal{G}_p(\beta g)e^{-\beta\Delta}$ with $\Delta = \omega - g\zeta(p)$ and $\mathcal{G}_p(\beta g)$ arising from thermal fluctuations and dependent on p .

For $p = 1$, Eq. (S6) at $k = 0$ diverges with N as $\tilde{J}_0 \approx \ln N + \gamma$, with γ the Euler-Mascheroni constant. We separate out this term in Eq. (S9). For $k \neq 0$, Eq. (S6) converges and we can use $\sum_{m=0}^{\infty} \cos(m\theta)/m = C_1(\theta) = -\ln|2\sin(\theta/2)|$. Hence

$$\ln Z \approx Ne^{-\beta\omega} \left(e^{\beta g(\ln N + \gamma)} + 2^{1-\beta g} N^{-1} \sum_{k=1}^{(N-1)/2} \left(\sin \frac{\pi k}{N} \right)^{-\beta g} \right), \quad (\text{S15})$$

where we have assumed N is odd for simplicity (assuming even N will give the same final result below). Noting that the sum is dominated by small k terms, we can use the small-angle approximation $\sin(\theta) \approx \theta$,

$$\begin{aligned} \ln Z &\approx Ne^{-\beta\omega} \left(e^{\beta g(\ln N + \gamma)} + \frac{1}{\pi} \left(\frac{N}{2\pi} \right)^{\beta g - 1} \sum_{k=1}^{(N-1)/2} k^{-\beta g} \right), \\ &\approx Ne^{-\beta(\omega - g(\ln N + \gamma))} \left(1 + \frac{2}{N} \left(\frac{1}{2\pi e^\gamma} \right)^{\beta g} \zeta(\beta g) \right), \\ &\approx Ne^{-\beta(\omega - g(\ln N + \gamma))}, \\ &= e^{-\beta\omega} e^{\beta g \gamma} N^{1+\beta g}. \end{aligned} \quad (\text{S16})$$

Hence for $p = 1$ fluctuations are suppressed for low temperatures and large N , and the dimensionless free energy is $\ln Z \approx Ne^{-\beta\Delta}$ with $\Delta \approx \omega - g(\ln N + \gamma)$. The low-temperature work output within this approximation is then (see Fig. S2),

$$W \approx N\omega_0(r-1) (e^{-\beta_H \Delta} - e^{-\beta_C \Delta}) \approx \omega_0(r-1) e^{-\beta_H \omega_0} e^{\beta_H g \gamma} N^{1+\beta_H g}. \quad (\text{S17})$$

Summarising, to lowest order in g/ω and for large N and β , we obtain the dimensionless free energies,

$$\ln Z \approx \begin{cases} \sqrt{\frac{1}{2\pi\beta g \zeta(p-2)}} e^{-\beta\Delta}, & p > 3, \\ \sqrt{\frac{1}{\pi\beta g(3+\ln\beta g)}} e^{-\beta\Delta}, & p = 3, \\ \frac{1}{3\beta g \zeta(2)} e^{-\beta\Delta}, & p = 2, \\ e^{-\beta\Delta}, & p = 1, \end{cases} \quad (\text{S18})$$

with $\zeta(s) = \sum_{m=1}^{\infty} 1/m^s$ the Riemann-zeta function and $\Delta(\omega) = \omega(1 - \omega_0 g/\omega g_c)$.

S.D. Calculation of entanglement

Within the quadratic approximation in the previous section, the first excited state is a state with one excitation uniformly spread across all spins,

$$|1\rangle = \frac{1}{\sqrt{N}} \sum_{i=1}^N \hat{\sigma}_+^{(i)} |0\rangle. \quad (\text{S19})$$

We consider a partition dividing the chain in half. The entanglement entropy with respect to this partition and state $|1\rangle$ is

$$\mathcal{S} = -\text{Tr}_R(\rho_L \ln \rho_L), \quad (\text{S20})$$

with $\rho_L = \text{Tr}_R(|1\rangle\langle 1|)$ and $\text{Tr}_{R(L)}$ a partial trace over states in the right(left) half of the chain. It is straightforward to show that this gives $\mathcal{S} = \ln(N/2)$.

For low temperatures, we can qualitatively describe the system by the thermal state

$$\rho_T^{01} = \frac{1}{1 + e^{-\beta\Delta}} (|0\rangle\langle 0| + e^{-\beta\Delta} |1\rangle\langle 1|), \quad (\text{S21})$$

where $\Delta = \omega(1 - g/g_c)$ within the quadratic approximation. The Peres-Horodecki criterion states that a separable density matrix has positive partial trace [S12, S13]. Hence, if the density matrix does not have positive partial trace, the state is entangled (“non-PPT entanglement”). Due to the symmetry of the partition and the state, a sufficient condition for ρ_T^{01} to exhibit non-PPT entanglement is $\text{Tr}(\hat{M} \otimes \hat{M} \rho_T^{01}) < 0$, with \hat{M} any Hermitian operator acting on either the left ($\hat{M} \otimes$) or right ($\otimes \hat{M}$) partition of the chain [S14]. We choose $\hat{M} \otimes \hat{M} = \prod_{i=1}^N \hat{m}_i$ with

$$\hat{m}_i = \frac{1}{(1 + \alpha)^{1/N}} \left[\frac{\hat{\mathcal{I}}}{2} - \hat{\sigma}_z^{(i)} - \alpha \left(\frac{\hat{\mathcal{I}}}{2} + \hat{\sigma}_z^{(i)} \right) \right], \quad (\text{S22})$$

with $\hat{\mathcal{I}}$ the identity operator and $\alpha > 0$ a parameter to be chosen. This gives

$$\text{Tr}(\hat{M} \otimes \hat{M} \rho_T^{01}) = \frac{1 - \alpha e^{-\beta \Delta}}{(1 + \alpha)(1 + e^{-\beta \Delta})}. \quad (\text{S23})$$

We can make $\text{Tr}(\hat{M} \otimes \hat{M} \rho_T^{01})$ arbitrarily close to $-(1 + e^{\beta \Delta})^{-1}$ by choosing α to be large ($\alpha \gg e^{\beta \Delta}$). This choice of \hat{M} gives negative $\text{Tr}(\hat{M} \otimes \hat{M} \rho_T^{01})$ and hence the state exhibits non-PPT entanglement.

S.E. Calculation of counterdiabatic drive

Here we derive Eq. 6 in the main text. We find the coefficients C_{ij} in $\hat{H}_{\text{cd}} = \sum_{ij(j \neq i)} C_{ij} \hat{\sigma}_x^{(i)} \hat{\sigma}_y^{(j)}$ by minimising the action

$$S = \text{Tr}(G(\hat{H}_{\text{cd}})^2), \quad (\text{S24})$$

with $G = \frac{\partial \hat{H}}{\partial t} + i[\hat{H}_{\text{cd}}, \hat{H}]$ [S15, S16]. Hence we need to solve

$$\frac{\partial S}{\partial C_{ij}} = 2 \text{Tr} \left(G \frac{\partial G}{\partial C_{ij}} \right) = 0. \quad (\text{S25})$$

For notational simplicity, we set $J_{ii} = C_{ii} = 0$. We have

$$\begin{aligned} G &= -\omega'(t) \sum_p \sigma_z^p - i\omega(t) \sum_{i,j,p} C_{ij} [\sigma_x^i \sigma_y^j, \sigma_z^p] - ig \sum_{i,j,p,q} C_{ij} J_{pq} \sigma_x^i [\sigma_y^j, \sigma_x^p \sigma_x^q], \\ &= -\omega'(t) \sum_p \sigma_z^p + \omega(t) \sum_{i,j,p} C_{ij} (\sigma_x^i \sigma_x^j \delta_{pj} - \sigma_y^i \sigma_y^j \delta_{pi}) - g \sum_{i,j,p,q} C_{ij} J_{pq} \sigma_x^i (\sigma_z^p \sigma_x^q \delta_{jp} + \sigma_x^p \sigma_z^q \delta_{jq}), \\ &= -\omega'(t) \sum_p \sigma_z^p + \omega(t) \sum_{i,j} C_{ij} (\sigma_x^i \sigma_x^j - \sigma_y^i \sigma_y^j) - 2g \sum_{i,p,q} J_{pq} C_{ip} \sigma_x^i \sigma_x^q \sigma_z^p. \end{aligned} \quad (\text{S26})$$

Hence

$$\frac{\partial G}{\partial C_{mn}} = \omega(t) (\sigma_x^m \sigma_x^n - \sigma_y^m \sigma_y^n) - 2g \sum_{\ell \neq n} J_{n\ell} \sigma_x^m \sigma_x^\ell \sigma_z^n. \quad (\text{S27})$$

We now want to calculate the trace of $G \partial G / \partial C_{mn}$ ($m \neq n$). Considering the three terms in G and the two terms in $\partial G / \partial C_{mn}$ gives a total of six terms. However three of these are zero, since the trace of terms with an odd number of spin-1/2 operators is zero. The three remaining terms are as follows.

Firstly,

$$\text{Tr} \left[g\omega'(t) \sum_p \sigma_z^p \sum_\ell J_{n\ell} \sigma_x^m \sigma_x^\ell \sigma_z^n \right] = 2^N \frac{g\omega'(t) J_{mn}}{16}. \quad (\text{S28})$$

Next,

$$\text{Tr} \left[\omega(t)^2 \sum_{p,q} C_{pq} (\sigma_x^p \sigma_x^q - \sigma_y^p \sigma_y^q) (\sigma_x^m \sigma_x^n - \sigma_y^m \sigma_y^n) \right] = 2^N \frac{\omega(t)^2 C_{mn}}{4}. \quad (\text{S29})$$

Finally,

$$\begin{aligned}
& \text{Tr} \left[g^2 \sum_{p,q,r(q,r \neq p)} J_{pq} C_{pr} \sigma_x^r \sigma_x^q \sigma_z^p \sum_{\ell \neq n} J_{n\ell} \sigma_x^m \sigma_x^\ell \sigma_z^n \right], \\
&= \text{Tr} \left[g^2 \sum_{p,q,r(q,r \neq p)} J_{pq} C_{pr} \sigma_x^r \sigma_x^q \sigma_z^p \sum_{\ell \neq n} J_{n\ell} \sigma_x^m \sigma_x^\ell \sigma_z^n \right], \\
&= \text{Tr} \left[g^2 \sum_{p,q} J_{pq} C_{pq} (\sigma_x^q)^2 \sigma_z^p \sum_{\ell \neq n} J_{n\ell} \sigma_x^m \sigma_x^\ell \sigma_z^n \right] + \text{Tr} \left[g^2 \sum_{p,q,r(\text{distinct})} J_{pq} C_{pr} \sigma_x^r \sigma_x^q \sigma_z^p \sum_{\ell \neq n} J_{n\ell} \sigma_x^m \sigma_x^\ell \sigma_z^n \right], \quad (\text{S30}) \\
&= 2^N \frac{g^2 \sum_q J_{nq} C_{nq} J_{nm}}{64} + \text{Tr} \left[g^2 \sum_{p,q,r(\text{distinct})} J_{pq} C_{pr} \sigma_x^r \sigma_x^q \sigma_z^p \sum_{\ell \neq m,n} J_{n\ell} \sigma_x^m \sigma_x^\ell \sigma_z^n \right], \\
&= 2^N \frac{g^2 \sum_q J_{mn} J_{nq} C_{nq}}{64} + 2^N \frac{g^2 \sum_{\ell \neq m,n} (J_{n\ell}^2 C_{mn} + J_{mn} J_{n\ell} C_{n\ell})}{64}, \\
&= 2^N \frac{g^2 (J_{mn} (JC)_{nn} + (J^2)_{nn} C_{mn} / 2 - J_{mn}^2 C_{mn})}{32}.
\end{aligned}$$

Combining terms gives the coupled linear equations that determine C_{mn} ,

$$g\omega'(t)J_{mn} + 2\omega(t)^2 C_{mn} + g^2(J_{mn}(JC)_{nn} + (J^2)_{nn}C_{mn}/2 - J_{mn}^2 C_{mn}) = 0. \quad (\text{S31})$$

This gives

$$C_{mn} = -\frac{g\omega'(t)J_{mn} + g^2 J_{mn}(JC)_{nn}}{2\omega(t)^2 + g^2(J^2)_{nn}/2 - g^2 J_{mn}^2}. \quad (\text{S32})$$

Multiplying both sides by $g^2 J_{nm}$ and summing over m gives

$$g^2(JC)_{nn} = -(g\omega'(t) + g^2(JC)_{nn})f_n, \quad (\text{S33})$$

with

$$f_n = \sum_m \frac{g^2 J_{mn}^2}{2\omega(t)^2 + g^2 [(J^2)_{nn}/2 - J_{mn}^2]}. \quad (\text{S34})$$

Equation (S33) can be rearranged to give

$$g^2(JC)_{nn} = -\frac{g\omega'(t)f_n}{1 + f_n}. \quad (\text{S35})$$

Substituting this into Eq. (S32) gives

$$C_{mn} = -\frac{g\omega'(t) \left(\frac{1}{1+f_n} \right) J_{mn}}{2\omega(t)^2 + g^2 [(J^2)_{nn}/2 - J_{mn}^2]}. \quad (\text{S36})$$

For an infinite chain with $J_{mn} = 1/|m - n|^p$, $(J^2)_{nn}/2 = \zeta(2p)$ with $\zeta(s)$ the Riemann zeta function and $f_n = f$ is independent of n . Furthermore, we find that for integer values of p we can evaluate f analytically using Mathematica (for example, for $p = 1$, $f = 1 - x \cot x$ with $x = g\pi/\sqrt{g^2\zeta(2) + 64\omega(t)^2}$). For nearest neighbour interactions, $f = g^2/\omega(t)^2$, and

$$C_{mn} = -\frac{g\omega'(t)}{2(\omega(t)^2 + g^2)} \delta_{n,m+1}. \quad (\text{S37})$$

- [S2] M. Kac, G. E. Uhlenbeck, and P. C. Hemmer, On the van der Waals theory of the vapor-liquid equilibrium. I. Discussion of a one-dimensional model, *J. Math. Phys.* **4**, 216 (1963).
- [S3] M. Kac and C. J. Thompson, Critical behavior of several lattice models with long-range interaction, *J. Math. Phys.* **10**, 1373 (1969).
- [S4] S. A. Cannas and F. A. Tamarit, Long-range interactions and nonextensivity in ferromagnetic spin models, *Phys. Rev. B* **54**, R12661 (1996).
- [S5] E. Gonzalez-Lazo, M. Heyl, M. Dalmonte, and A. Angelone, Finite-temperature critical behavior of long-range quantum Ising models, *SciPost Phys.* **11**, 76 (2021).
- [S6] J. Zhang, G. Pagano, P. W. Hess, A. Kyprianidis, P. Becker, H. Kaplan, A. V. Gorshkov, Z.-X. Gong, and C. Monroe, Observation of a many-body dynamical phase transition with a 53-qubit quantum simulator, *Nature* **551**, 601 (2017).
- [S7] T. Holstein and H. Primakoff, Field dependence of the intrinsic domain magnetization of a ferromagnet, *Phys. Rev.* **58**, 1098 (1940).
- [S8] M. Vogl, P. Laurell, H. Zhang, S. Okamoto, and G. A. Fiete, Resummation of the Holstein-Primakoff expansion and differential equation approach to operator square roots, *Phys. Rev. Research* **2**, 043243 (2020).
- [S9] J. König and A. Hucht, Newton series expansion of bosonic operator functions, *SciPost Phys.* **10**, 007 (2021).
- [S10] L. Cevolani, G. Carleo, and L. Sanchez-Palencia, Spreading of correlations in exactly solvable quantum models with long-range interactions in arbitrary dimensions, *New J. Phys.* **18**, 093002 (2016).
- [S11] J. Wu, X. Zhang, and D. Liu, An efficient calculation of the Clausen functions $\text{Cl}_n(\theta)$ ($n \geq 2$), *BIT Numer. Math.* **50**, 193 (2010).
- [S12] A. Peres, Separability criterion for density matrices, *Phys. Rev. Lett.* **77**, 1413 (1996).
- [S13] M. Horodecki, P. Horodecki, and R. Horodecki, Separability of mixed states: necessary and sufficient conditions, *Phys. Lett. A* **223**, 1 (1996).
- [S14] G. Tóth and O. Gühne, Entanglement and permutational symmetry, *Phys. Rev. Lett.* **102**, 170503 (2009).
- [S15] D. Sels and A. Polkovnikov, Minimizing irreversible losses in quantum systems by local counterdiabatic driving, *Proc. Natl. Acad. Sci. U.S.A.* **114**, E3909 (2017).
- [S16] M. Kolodrubetz, D. Sels, P. Mehta, and A. Polkovnikov, Geometry and non-adiabatic response in quantum and classical systems, *Phys. Rep.* **697**, 1 (2017).